A Sliding Mode Control Law for Epipolar Visual Servoing of Differential-Drive Robots

H. M. Becerra and C. Sagues

Abstract— **In this paper, a robust control technique (Sliding Mode Control) is proposed to be used in order to perform visual servoing for differential-drive mobile robots using the classical teach-by-showing strategy. We propose a commuted sliding mode control law that exploits the epipolar geometry. The major contribution of the paper is the design of a control law that solves the problem of passing through a singularity induced by the epipoles maintaining bounded inputs. Moreover, the designed control is able to drive the robot to the target even when it just starts on the singularity. The proposed approach does not need a precise camera calibration due to the robustness of the control system under uncertainty in parameters. It also ensures entire correction of both orientation and lateral error even with noise in the image. The effectiveness of our approach is tested via simulations.**

I. INTRODUCTION

A vision system can provide a lot of information from the environment and making use of this information cannot be an easy task. The viability of using a vision system in control of robots has been well studied [1]. Specially, incorporating machine vision in mobile robots can improve their navigation capabilities [2].

Nowadays the research on visual servoing tries about applications on monocular vision. On this context, a good way to extract useful information in order to control a robot is by means of geometric constraints that relate two images. Geometric constraints are imposed on images when there exist correspondences between features [3]. Two constraints are well known: epipolar geometry and the homography model. Their application, without their decomposition, is classified as the so-called image-based visual servoing. Currently, this approach has shown to be the best option in comparison with the position-based visual servoing. In the image-based approach the visual control is performed directly in the image space. Examples of image-based methods are [4], [5], [6]. Some contributions combining position-based and image-based approaches have been performed as well [7], [8], [9].

Epipolar geometry has been applied in some works [10], [11], [12], [13]. These works deal with the teach-by-showing problem, where a reference image is used to define the desired pose (position and orientation) of an on-board camera. This target pose should be reached using only image data provided from the current and target images. In [10] is reported a visual servoing based on epipolar geometry for manipulators. In [11] a epipolar-based visual servoing for nonholonomic mobile robots is introduced. This approach takes into account the nonholonomic nature of the robot by driving the epipoles to zero in a smooth way; however, the resulting motion steers the robot away from the target while the lateral error is corrected and after that, the robot moves forwards in an straight line to the target position. [12] presents a more intuitive way to drive the robot directly towards the target. The approach in [13] is an outgrowth of [11]. In [13], zeroing the epipoles is viewed like an stabilization problem of the epipolar system, unlike the tracking problem in [11]. Epipolar geometry has the drawback that degenerates with short baseline and becomes ill-conditioned for planar scenes. This problem can be overcome by using feature-based strategies or by switching to a homography-based control once epipolar geometry begins to degenerate [14].

Our work focuses in exploiting the epipolar geometry on the basis of image-based visual servoing. We propose a commuted sliding mode control law in order to steer a differential-drive mobile robot using a teach-by-showing strategy. The main contribution of the paper is that the designed control law solves the problem of passing through a singularity caused by the epipolar geometry using bounded control inputs. Moreover, the visual control can be performed even when the initial robot pose is just on the singular point. The designed control law does not need a precise calibration of the vision system due to its intrinsic robustness under parameters uncertainty and matched disturbances. Our approach ensures total correction of both orientation and lateral error.

The paper is organized as follows. Section II introduces some basic background of sliding mode control theory. Section III specifies the mathematical modeling that is used for the visual sensor and the mobile robot. Section IV details the design procedure for the sliding mode control law. Section V presents the stability and robustness analysis. Section VI shows the performance of the closed-loop control system via simulations and finally, Section VII provides the conclusions.

II. BASICS OF SLIDING MODE CONTROL

Sliding Mode Control (SMC) is gaining importance as a universal design methodology for the robust control of linear and nonlinear systems. It offers several redeeming features from a control theory point of view [15], namely, an inherent order reduction, direct incorporation of robustness against system uncertainties and disturbances, and an implicit stability proof.

This work was supported by projects DPI 2006-07928, IST-1-045062-URUS-STP and grants of Banco Santander-Univ. Zaragoza and Conacyt-México.

H.M. Becerra and C. Sagues are with DIIS, Universidad de Zaragoza C/ María de Luna 1, E-50018 Zaragoza, Spain {hector.becerra, csagues}@unizar.es

Basically, SMC makes use of a high-speed switching control law to drive the nonlinear state trajectory of the system onto a specified and user-chosen surface in the state space (called the sliding or switching surface) in a finite time, and to keep the state trajectory on this surface for all subsequent time. The plant dynamics constrained to this surface represent the controlled system's behavior, which is independent of matched uncertainties and disturbances. Matched uncertainties are those that belong to the range space of the input vector. This is the so-called matching condition.

Sliding modes are well studied in a class of systems having a state model nonlinear in the state vector $\mathbf{x}(\cdot)$ and linear in the control vector $\mathbf{u}(\cdot)$ (affine systems) of the form

$$\dot{\mathbf{x}} = f(t, \mathbf{x}, \mathbf{u}) = f(t, \mathbf{x}) + B(t, \mathbf{x})\mathbf{u} \tag{1}$$

where the state vector $\mathbf{x}(t) \in \Re^n$, the control vector $\mathbf{u}(t) \in \Re^m$, $f(t, \mathbf{x}) \in \Re^n$, and $B(t, \mathbf{x}) \in \Re^{n \times m}$.

The *switching surface* is so called because if the state trajectory of the system is "above" the surface, then the control input has one gain, and a different gain is applied if the trajectory drops "below" the surface. Thus, each entry $u_i(t)$ of the switched control $\mathbf{u}(t) \in \Re^m$ has the form

$$u_i(t, \mathbf{x}) = \left\{ \begin{array}{ll} u_i^+(t, \mathbf{x}) & \text{if } s_i(\mathbf{x}) > 0 \\ u_i^-(t, \mathbf{x}) & \text{if } s_i(\mathbf{x}) < 0 \end{array} \right\}, i = 1, ..., m \tag{2}$$

where $s_i = 0$ is the i-th switching surface associated with $\mathbf{s}(\mathbf{x}) = \left[\begin{array}{ccc} s_1(\mathbf{x}) & \cdots & s_m(\mathbf{x}) \end{array} \right]^T = \mathbf{0}$, the $(n-m)$-dimensional switching surface.

SMC design breaks down into two phases. Phase one implies constructing switching surfaces so that the system restricted to these surfaces produces a desired behavior. Phase two involves constructing switched feedback gains which drive the state trajectory to the sliding surface maintaining it there.

An undesirable phenomenon presented in SMC systems is the chattering. This is an oscillation within a neighborhood of the switching surface such that $\mathbf{s}(\mathbf{x}) = \mathbf{0}$ is not satisfied for all time after the switching surface is reached. If the frequency of the switching is very high compared with the dynamic response of the system the chattering problem is often but not always negligible.

III. MATHEMATICAL MODELING

A. Visual Sensing

Consider the geometry of the camera to be modeled by perspective projection, where the internal camera calibration matrix is as follows

$$\mathbf{K} = \left[\begin{array}{ccc} \alpha_x & s & x_0 \\ 0 & \alpha_y & y_0 \\ 0 & 0 & 1 \end{array} \right] \tag{3}$$

where α_x and α_y represent the focal length of the camera in terms of pixel dimensions in the x and y direction respectively, s is the skew parameter and $(x_0,\ y_0)$ are the coordinates of the principal point. We have that $\alpha_x = fm_x$ and $\alpha_y = fm_y$, where f is the focal length in distance units and m_x, m_y are the pixels per distance unit. We assume that the principal point is in the center of the image ($x_0 = 0$, $y_0 = 0$) and there is no skew ($s = 0$).

B. Robot Kinematics

The system to be controlled is a differential-drive robot, whose kinematic model is consistent with the general affine system in (1). The differential kinematics of the robot expressed in state space is as follows

$$\left[\begin{array}{c} \dot{x} \\ \dot{z} \\ \dot{\phi} \end{array} \right] = \left[\begin{array}{cc} -\sin\phi & 0 \\ \cos\phi & 0 \\ 0 & 1 \end{array} \right] \left[\begin{array}{c} v \\ \omega \end{array} \right]. \tag{4}$$

Thus, $\mathbf{x} = (x, z, \phi)^T$ represents the state of the robot system, where $x(t)$ and $z(t)$ are the robot position in the plane, $\phi(t)$ is the robot orientation, expressed as the angle between the robot body-fixed z-axis and the world z-axis, and $v(t)$ and $\omega(t)$ are the translational and angular input velocities, respectively. v is in the direction of the robot body-fixed z-axis and ω is about the robot y-axis, i.e. rotation in the plane.

According to the general affine system in (1), the model (4) presents the particularity that $f(t, \mathbf{x}) = \mathbf{0}$ and consequently, this is a driftless system. Furthermore, the corresponding linear approximation in any point $\mathbf{x}(t) \in \Re^n$ is uncontrollable. However, it fulfills the Lie Algebra rank condition [16], in such a way that controllability can be demonstrated.

Let us define the outputs of the system using the x-coordinates of the epipoles for the current (e_{cx}) and target (e_{tx}) images. The epipoles can be expressed as a function of the state of the robot

$$\begin{array}{rcl} e_{cx} & = & \alpha_x \dfrac{x\cos\phi + z\sin\phi}{z\cos\phi - x\sin\phi}, \\ e_{tx} & = & \alpha_x \dfrac{x}{z}. \end{array} \tag{5}$$

Then, the two-dimensional output of the system is

$$\mathbf{y} = h(\mathbf{x}) = \left[\begin{array}{cc} e_{cx} & e_{tx} \end{array} \right]^T. \tag{6}$$

Cartesian coordinates x and z can be expressed as a function of the polar coordinates d and ψ as

$$x = -d\sin\psi, \quad z = d\cos\psi, \tag{7}$$

with $\psi = -\arctan(e_{tx}/\alpha_x)$, $\phi - \psi = \arctan(e_{cx}/\alpha_x)$ and $d^2 = x^2 + z^2$.

IV. SLIDING MODE CONTROL LAW DESIGN

The objective is to perform the navigation by using the feedback information provided by the x-coordinate of the epipoles. Like in previous works in the area ([11], [12]), the visual servoing problem is transformed in a tracking problem for a nonlinear system, where the reference trajectories for the epipoles are defined. Unlike these works, a robust tracking under uncertainty of parameters is an issue to be

improved. We propose to perform a smooth motion towards the target position by using sinusoidal desired trajectories to drive the epipoles to zero. The main concern is to face the singularity problem that in [13] is evaded regardless, and in [14] they avoid to compute control inputs at the singular point. The singularity appears due to the decoupling matrix of the system becomes singular in a point of the state trajectory. Particularly, the singularity causes the translational velocity growing up without a limit when the system evolves near to the singular point. We solve it by switching to a bounded SMC law to pass through the singularity.

Let us define the tracking error system (ξ-system) using the change of variables $\xi_c = e_{cx} - e^d_{cx}$, $\xi_t = e_{tx} - e^d_{tx}$ and the polar coordinates in (7).

$$\begin{bmatrix} \dot{\xi}_c \\ \dot{\xi}_t \end{bmatrix} = \begin{bmatrix} -\frac{\alpha_x \sin(\phi-\psi)}{d\cos^2(\phi-\psi)} & \frac{\alpha_x}{\cos^2(\phi-\psi)} \\ -\frac{\alpha_x \sin(\phi-\psi)}{d\cos^2(\psi)} & 0 \end{bmatrix} \begin{bmatrix} \upsilon \\ \omega \end{bmatrix} - \begin{bmatrix} \dot{e}^d_{cx} \\ \dot{e}^d_{tx} \end{bmatrix}. \tag{8}$$

The system (8) has the form $\dot{\xi} = \mathbf{M}(\phi,\psi)\mathbf{u} - \dot{\mathbf{e}}^d$, where $\mathbf{M}(\phi,\psi)$ corresponds to the decoupling matrix and $\dot{\mathbf{e}}^d$ represents a known disturbance. It is evident that the decoupling matrix loses rank if $\phi - \psi = n\pi$ with $n \in \mathbb{Z}$. For all the rest of the state space this matrix is invertible, with inverse matrix

$$\mathbf{M}^{-1}(\phi,\psi) = \frac{1}{\alpha_x} \begin{bmatrix} 0 & -\frac{d\cos^2(\psi)}{\sin(\phi-\psi)} \\ \cos^2(\phi-\psi) & -\cos^2(\psi) \end{bmatrix}. \tag{9}$$

We faced the tracking problem as an stabilization problem of the error system (8).

A. Decoupling-based Control Law

1) First Stage: The simplest form to define sliding surfaces in the ξ-system is directly to take the errors as sliding surfaces, in such a way that if there exist switched feedback gains that make the states to evolve in $\mathbf{s} = 0$, then the tracking problem is solved.

$$\mathbf{s} = \begin{bmatrix} s_c \\ s_t \end{bmatrix} = \begin{bmatrix} \xi_c \\ \xi_t \end{bmatrix} = \begin{bmatrix} e_{cx} - e^d_{cx} \\ e_{tx} - e^d_{tx} \end{bmatrix}. \tag{10}$$

2) Second Stage: This stage uses the sliding surfaces already defined and the *equivalent control method* in order to find switched feedback gains to drive the state trajectory to $\mathbf{s} = 0$ and maintain it there.

The equivalent control method consist of working out the value of inputs from the equation $\dot{\mathbf{s}} = 0$. The so-called equivalent control is then

$$\mathbf{u}_{eq} = \mathbf{M}^{-1}(\phi,\psi)\dot{\mathbf{e}}^d. \tag{11}$$

A decoupling-based SMC law that ensures global stabilization of the ξ-system has the form $\mathbf{u}_{sm} = \mathbf{u}_{eq} + \mathbf{u}_{disc}$, where $\mathbf{u}_{disc}$ is a two-dimensional vector containing switched feedback gains. We propose the simplest form of these gains as follows

$$\mathbf{u}_{disc} = \mathbf{M}^{-1}(\phi,\psi) \begin{bmatrix} -k^{sm}_c sign(s_c) \\ -k^{sm}_t sign(s_t) \end{bmatrix} \tag{12}$$

where $k^{sm}_c > 0$ and $k^{sm}_t > 0$ are control gains. In spite of $\mathbf{u}_{sm}$ can achieve global stabilization of the ξ-system, it needs high gains and it does not reach the sliding surfaces in a smooth way. It can cause a non-smooth behavior in the robot state that is not valid in real situations. To alleviate this issue we add a pole placement term in the control law

$$\mathbf{u}_{pp} = \mathbf{M}^{-1}(\phi,\psi) \begin{bmatrix} -k_c & 0 \\ 0 & -k_t \end{bmatrix} \begin{bmatrix} \xi_c \\ \xi_t \end{bmatrix} \tag{13}$$

where $k_c > 0$ and $k_t > 0$ are control gains. Finally, the complete SMC law that achieves robust global stabilization of the system (8) is as follows

$$\mathbf{u}_{db} = \begin{bmatrix} \upsilon_{db} & \omega_{db} \end{bmatrix}^T = \mathbf{u}_{eq} + \mathbf{u}_{disc} + \mathbf{u}_{pp}. \tag{14}$$

B. Bounded Control Law

The control law in (14) utilizes the decoupling matrix and it presents the singularity problem for the condition $e_{cx} = 0$ ($\phi - \psi = n\pi$ with $n \in \mathbb{Z}$), which means that the camera axis of the robot at its current pose is aligned with the baseline. We can note from (9) that the singularity only affects the translational velocity computation. In order to pass through this singularity we propose to commute to a direct sliding mode controller when $\phi - \psi$ is near to $n\pi$. This kind of controller has been studied for output tracking through singularities [17]. The direct sliding mode controller is as follows

$$\mathbf{u}_b = \begin{bmatrix} \upsilon_b \\ \omega_b \end{bmatrix} = \begin{bmatrix} -M sign\left(s_t\ b\left(\phi,\psi\right)\right) \\ -N sign(s_c) \end{bmatrix} \tag{15}$$

where M and N are suitable gains and $b\left(\phi,\psi\right)$ is a function that describes the change in sign of the translational velocity when the state trajectory crosses the singularity. We can find out this function from (8) as follows

$$\begin{aligned} \dot{\xi}_c &= b_1\left(\phi,\psi\right)\upsilon + b_2\left(\phi,\psi\right)\omega - \dot{e}^d_{cx}, \\ \dot{\xi}_t &= b_3\left(\phi,\psi\right)\upsilon - \dot{e}^d_{tx} \end{aligned} \tag{16}$$

where $b_1 = -\frac{\alpha_x \sin(\phi-\psi)}{d\cos^2(\phi-\psi)}$, $b_2 = \frac{\alpha_x}{\cos^2(\phi-\psi)}$, $b_3 = -\frac{\alpha_x \sin(\phi-\psi)}{d\cos^2(\psi)}$. According to that, b_2 is always positive, and $sign(b_1) = sign(b_3) = sign(-\sin(\phi-\psi))$. Hence,

$$b\left(\phi,\psi\right) = -\sin(\phi-\psi). \tag{17}$$

The control law in (15) with $b\left(\phi,\psi\right)$ as in (17) locally stabilizes the system (8) and is always bounded.

C. Desired Trajectories for the Epipoles

The desired trajectories must provide a smooth zeroing of the epipoles from their initial values as main requirement. We can see from Fig. 1 how a natural zeroing of epipoles is produced when robot performs a smooth direct motion from an initial pose where $sign\left(e_{cx}\right) \neq sign\left(e_{tx}\right)$ towards the target, but not when robot has an initial pose where $sign\left(e_{cx}\right) = sign\left(e_{tx}\right)$. In order to drive the epipoles to zero from a pose where the last happens (Fig. 1(b)), the robot has firstly to reach a pose where $sign\left(e_{cx}\right) \neq sign\left(e_{tx}\right)$ (Fig. 1(a)). Thus, we define desired trajectories which are always opposite in sign each other.

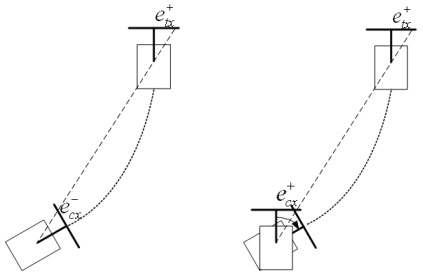

(a) (b)

Fig. 1. (a) $sign\,(e_{tx}) \neq sign\,(e_{cx})$ - direct motion towards the target, (b) $sign\,(e_{tx}) = sign\,(e_{cx})$ - reaching the same condition as in (a).

$$\begin{aligned} e^d_{cx}\,(t) &= S\frac{e_{cx}(0)}{2}\left(1+\cos\left(\frac{\pi}{T}t\right)\right),\ 0 \leq t \leq T \quad (18)\\ e^d_{cx}\,(t) &= 0, \qquad\qquad\qquad\qquad T < t < \infty \end{aligned}$$

$$\begin{aligned} e^d_{tx}\,(t) &= \frac{e_{tx}(0)}{2}\left(1+\cos\left(\frac{\pi}{T}t\right)\right), \quad 0 \leq t \leq T\\ e^d_{tx}\,(t) &= 0, \qquad\qquad\qquad\qquad T < t < \infty \end{aligned}$$

where $S = -sign\,(e_{cx}(0)e_{tx}(0))$ and T is the time to reach epipoles to zero.

V. STABILITY AND ROBUSTNESS ANALYSIS

When epipoles reach to zero the so-called *zero dynamics* in the robot system is achieved. Zero dynamics is described by a subset of the state space which makes the output to be identically zero [18]. In the particular case of the robot system (4) with output vector (6), this set is given as follows

$$\begin{aligned} Z^* &= \left\{\begin{bmatrix} x & z & \phi \end{bmatrix}^T \mid e_{cx} = 0,\ e_{tx} = 0\right\} \quad (19)\\ &= \left\{\begin{bmatrix} 0 & z & 0 \end{bmatrix}^T,\ z \in \mathbb{R}\right\}. \end{aligned}$$

Zero dynamics in this control system means that when epipoles are zero, the x-coordinate and the orientation of the robot are corrected, but depth may be different to zero. Once the relationship between zeroing the epipoles and the robot state is established, we focus on demonstrating stability and robustness for the tracking control law.

Proposition 1. A commuted control law that combines the decoupling-based control in (14) by switching to the bounded control in (15) whenever $|\phi - \psi| < n\pi + T_h$, where T_h is a suitable threshold value and $n \in \mathbb{Z}$, achieves global stabilization of the system in (8). Moreover, global stabilization is achieved even with uncertainty in parameters.

Proof: Stabilization of (8) is proved by showing that the sliding surfaces can be reached in a finite time (existence conditions of sliding modes). Let be the natural Lyapunov function for a sliding mode controller

$$V = V_1 + V_2, \quad V_1 = \frac{1}{2}s_c^2, \quad V_2 = \frac{1}{2}s_t^2 \qquad (20)$$

which accomplish $V(s_c = 0,\ s_t = 0) = 0$ and $V > 0$ for all $s_c \neq 0,\ s_t \neq 0$.

$$\dot{V} = \dot{V}_1 + \dot{V}_2 = s_c\dot{s}_c + s_t\dot{s}_t. \qquad (21)$$

We analyze each term of (21) for the decoupling-based controller in (14)

$$\begin{aligned} \dot{V}_1 &= s_c\left(-\frac{\alpha_x}{\alpha_{x_e}}\left(k_c^{sm}sign\,(s_c) + k_c s_c\right) + A\right)\\ &= -\left(\frac{\alpha_x}{\alpha_{x_e}}\left(k_c^{sm}\,|s_c| + k_c s_c^2\right) - s_c A\right),\\ \dot{V}_2 &= s_t\left(-\frac{\alpha_x d_e}{\alpha_{x_e} d}\left(k_t^{sm}sign(s_t) + k_t\xi_t\right) + B\right)\\ &= -\left(\frac{\alpha_x d_e}{\alpha_{x_e} d}\left(k_t^{sm}\,|s_t| + k_t s_t^2\right) - s_t B\right) \end{aligned}$$

where $B = \left(\frac{\alpha_x d_e}{\alpha_{x_e} d} - 1\right)\dot{e}^d_{tx}$, $A = \frac{\alpha_x}{\alpha_{x_e}}\left(\frac{d_e}{d} - 1\right)\left(\dot{e}^d_{tx} - k_t^{sm}sign(s_t) - k_t s_t\right)\frac{\cos^2(\psi)}{\cos^2(\phi-\psi)} + \left(\frac{\alpha_x}{\alpha_{x_e}} - 1\right)\dot{e}^d_{cx}$, and α_{x_e}, d_e represent estimated values for the corresponding system parameter. We can see that

$$\begin{aligned} \dot{V}_1 &\leq -\left(\frac{\alpha_x}{\alpha_{x_e}}\left(k_c^{sm} + k_c\,|s_c|\right) - |A|\right)|s_c|,\\ \dot{V}_2 &\leq -\left(\frac{\alpha_x d_e}{\alpha_{x_e} d}\left(k_t^{sm} + k_t\,|s_t|\right) - |B|\right)|s_t|. \end{aligned}$$

$\dot{V}_1$ and $\dot{V}_2$ are negative definite iff the following inequalities are guaranteed for all $s_c \neq 0,\ s_t \neq 0$

$$\begin{aligned} k_c^{sm} + k_c\,|s_c| &> \frac{\alpha_{x_e}}{\alpha_x}|A|, \qquad (22)\\ k_t^{sm} + k_t\,|s_t| &> \frac{\alpha_{x_e} d}{\alpha_x d_e}|B|. \end{aligned}$$

Therefore, $\dot{V} < 0$ iff both inequalities in (22) are fulfilled. Global convergence to the sliding surfaces can be achieved regardless of uncertainty in parameters.

Now, let develop the existence conditions of sliding modes for the bounded controller (15). The same Lyapunov function in (20) is used. For each term of (21) after some basic operations we have

$$\begin{aligned} \dot{V}_1 &= -N\frac{\alpha_x}{\cos^2(\phi-\psi)}|s_c| - s_c\dot{e}^d_{cx} - s_c C,\\ \dot{V}_2 &= -M\frac{\alpha_x\,|b\,(\phi,\psi)|}{d\cos^2(\psi)}|s_t| - s_t\dot{e}^d_{tx} \end{aligned}$$

where $C = M\frac{\alpha_x|b(\phi,\psi)|}{d\cos^2(\phi-\psi)}sign(s_t)$ and $b\,(\phi,\psi)$ is given in (17). We can see that

$$\begin{aligned} \dot{V}_1 &\leq -\left(N\frac{\alpha_x}{\cos^2(\phi-\psi)} - \left|\dot{e}^d_{cx}\right| - |C|\right)|s_c|,\\ \dot{V}_2 &\leq -\left(M\frac{\alpha_x\,|b\,(\phi,\psi)|}{d\cos^2(\psi)} - \left|\dot{e}^d_{tx}\right|\right)|s_t|. \end{aligned}$$

$\dot{V}_1$ and $\dot{V}_2$ are negative definite iff the following inequalities are assured for all $s_c \neq 0,\ s_t \neq 0$

$$\begin{aligned} N &> \frac{\cos^2(\phi-\psi)}{\alpha_x}\left(|C| + \left|\dot{e}^d_{cx}\right|\right), \qquad (23)\\ M &> \frac{d\cos^2(\psi)}{\alpha_x\,|b\,(\phi,\psi)|}\left|\dot{e}^d_{tx}\right|. \end{aligned}$$

Therefore, $\dot{V} < 0$ iff both inequalities in (23) are fulfilled. The bounded controller does not need any information of system parameters and thus, its robustness is implicit.

According to the existence conditions of sliding modes, the bounded controller (15) is able to locally stabilize the system (8); its region of attraction is bigger as long as the control gains M and N are higher. Nevertheless, this controller can not achieve the smooth behavior demanded for real situations and it is only used to cross the singularity. Due to the control strategy commutes between two switching control laws and each one acts inside of its region of attraction, respectively, the commutation between the control laws does not affect the stability of the control system. The decoupling-based controller ensures entering to the region of attraction of the bounded one.

Once sliding surfaces are reached for any case of SMC law, the system's behavior is independent of matches uncertainties and disturbances. It is clear that uncertainties in the system (8) fulfill the matching condition and as a result, robustness of the control system is accomplished. ■

VI. SIMULATION RESULTS

In this section, we present some simulations of the control system as is established in the Proposition 1. Simulations have been performed in Matlab/Simulink. Results show how the main objective of driving the robot to a desired pose ((0,0,0^o) in all the cases) is attained regardless of passing through the singularity, and moreover, the task is accomplished even when the robot starts in a pose where singularity occurs. Simulations also show the good performance of the approach under uncertainty in parameters and image noise.

In the first simulations, it is assumed the camera is calibrated in advance. We used a focal length (f) of 6 mm, an initial distance between the current and target positions (d) of 12 m, a virtual image size of 640×480 pixels. Related to the controllers, the time to reach the target (T) is fixed to 100 s, the threshold to switch to the bounded control law (T_h) is fixed to 0.03 rad and the control gains are set to $k_c = 0.4$, $k_t = 0.6$, $k_c^{sm} = 10$, $k_t^{sm} = 2$, $M = 0.5$, $N = 0.4$.

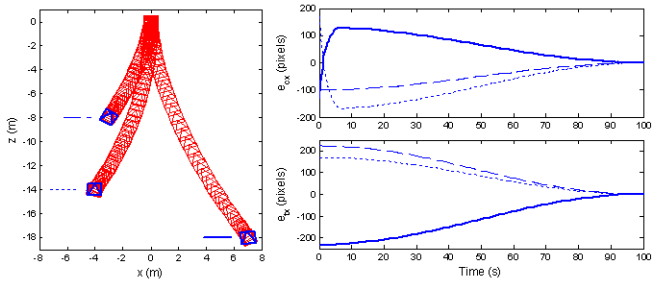

(a) (b)

Fig. 2. Resultant paths and evolution of epipoles for three non-singular initial poses. (a) Paths on the $x - z$ plane. (b) Current and target epipoles.

Fig. 2 shows paths and epipoles evolution for initial poses (-3,-8,-30^o), (-4,-14,0^o) and (7,-18,9^o). In the two last cases, the robot starts with $sign\,(e_{cx}) = sign\,(e_{tx})$ and epipoles are taken to the opposite-signed trajectories. In both cases e_{cx} changes its sign during the first seconds, which causes a rotation to the robot, and then, it begins a direct motion towards the target. Note that the state trajectory crosses the singularity $e_{cx} = 0$ for the initial cases (-4,-14,0^o) and (7,-18,9^o). This is performed using bounded input velocities, as can be seen in Fig. 3, where state variables evolution and control inputs are shown for the initial pose (7,-18,9^o). It is worth noting that the control inputs are maintained bounded even when the epipoles reach to zero after 100 s, which ensures entire correction of orientation and lateral position.

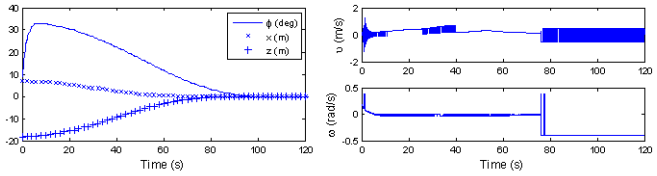

(a) (b)

Fig. 3. Evolution of the position and orientation of the robot and control inputs for a case where the singularity is crossed. (a) Position and orientation. (b) Control inputs.

In Fig. 4(a) we present paths for two special cases where the state trajectory just starts on the singularity $e_{cx} = 0$. The drawn line from the robot initial position to the target shows that the camera axis is aligned with the baseline for that pose. In these cases, we assign a suitable amplitude to the desired trajectory for the current epipole. Due to $|\phi - \psi|$ is less than the threshold, the bounded controller takes the system out of the singularity and then, the epipoles evolve as is shown in Fig. 4(b).

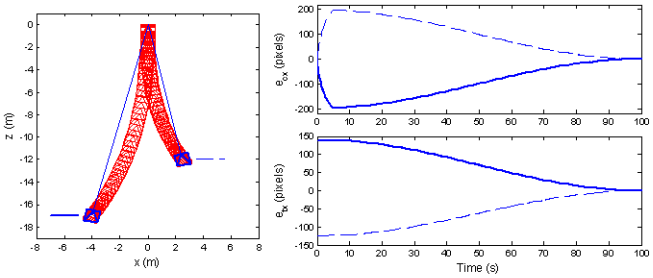

(a) (b)

Fig. 4. Resultant paths and evolution of epipoles for two singular initial poses. (a) Paths on the $x - z$ plane. (b) Current and target epipoles.

In order to show the robustness of the control law under uncertainty in parameters f and d, we include Fig. 5 and Table I. In the control law these parameters are fixed to $f = 6$ mm and $d = 12$ m. Focal length is changed in the computation of epipoles and different initial positions are tested to change d. Table I presents the mean squared tracking errors for different values of the parameters. As well as tracking error is maintained in a small value, the robot goes to the target in all the cases.

Finally, Fig. 6 shows the performance of the approach under image noise for initial pose (-7,-20,-12^o). The added noise has a standard deviation of 1 pixel and the time to

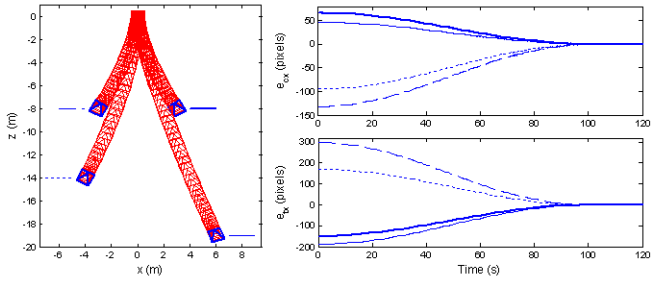

(a) (b)

Fig. 5. Resultant paths and evolution of epipoles with variation of parameters f and d. (a) Paths on the $x-z$ plane. (b) Current and target epipoles.

TABLE I

MEAN SQUARED TRACKING ERRORS FOR DIFFERENT PARAMETERS.

	$f=4$ $d=8.54$	$f=6$ $d=8.54$	$f=8$ $d=8.54$	$f=6$ $d=14.56$	$f=6$ $d=19.92$
	(3,-8,30)	(-3,-8,-30)	(-3,-8,-30)	(-4,-14,-25)	(6,-19,22)
ξ_c	0.01	0.19	0.41	0.26	0.38
ξ_t	0.004	0.61	3.23	0.002	0.13

reach the target is set to 120 s. Orientation and x-position are corrected effectively; however, the robot autonomously performs a motion to attain the control objective (track the desired trajectories for the epipoles). Therefore, orientation and lateral errors can be always corrected successfully, but depth may be different to zero. There exist methods that can be used to eliminate the final depth error ([10], [14]).

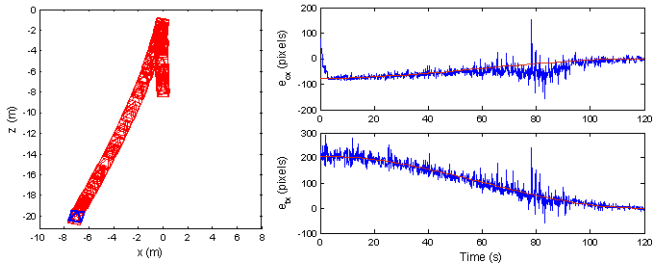

(a) (b)

Fig. 6. Resultant paths and epipoles evolution adding noise to a virtual image. (a) Paths on the $x-z$ plane. (b) Current and target epipoles.

VII. CONCLUSIONS

In this work, a robust control law is presented in order to perform image-based visual servoing for differential-drive mobile robots. The visual control utilizes the usual teach-by-showing strategy. We propose a sliding mode control law, which exploits the epipolar geometry between a current image and a target one without requiring any a prior knowledge of the scene or precise camera calibration due to the intrinsic robustness of the control law against matched uncertainties and disturbances.

Our major contribution is that the designed control law solves the problem of passing through the singularity induced by the epipoles maintaining bounded inputs. Furthermore, the visual control accomplishes its goal even when the robot starts on the singularity. We face the visual servoing task as the problem of zeroing the epipoles by means of tracking suited sinusoidal trajectories. The control law consists of two sliding mode controllers; the first one is based on decoupling the system, and acts when state trajectory is away from the singularity, and the second one is a bounded control, which acts near the singular point in order to pass through it or to keep the control when the robot is reaching the target pose. Simulations have proven the good performance of the method to ensure orientation and lateral position correction even with noise in the image.

REFERENCES

[1] S. Hutchinson, G.D. Hager, and P.I. Corke. A tutorial on visual servo control. *IEEE Transactions on Robotics and Automation*, 12(5):651–670, 1996.

[2] G.N. DeSouza and A.C. Kak. Vision for mobile robot navigation: A survey. *IEEE Trans. on Patt. Analysis and Machine Intelligence*, 24(2):237–267, 2002.

[3] R. Hartley and A. Zisserman. *Multiple View Geometry in Computer Vision*. Cambridge University Press, Cambridge, 2000.

[4] Y. Ma, J. Kosecka, and S. Sastry. Vision guided navigation for a nonholonomic mobile robot. *IEEE Transactions on Robotics and Automation*, 15(3):521–537, 1999.

[5] S. Benhimane and E. Malis. Homography-based 2D visual servoing. In *IEEE International Conference on Robotics and Automation*, pages 2397–2402, 2006.

[6] G. López-Nicolás, C. Sagüés, and J.J. Guerrero. Homography-based visual control of nonholonomic vehicles. In *IEEE International Conference on Robotics and Automation*, pages 1703–1708, 2007.

[7] E. Malis, F. Chaumette, and S. Boudet. 2 1/2 D visual servoing. *IEEE Transactions on Robotics and Automation*, 15(2):234–246, April 1999.

[8] Y. Fang, W. E. Dixon, D. M. Dawson, and P. Chawda. Homography-based visual servo regulation of mobile robots. *IEEE Transactions on Systems, Man, and Cybernetics, Part B*, 35(5):1041–1050, 2005.

[9] G. López-Nicolás, S. Bhattacharya, J.J. Guerrero, C. Sagüés, and S. Hutchinson. Switched homography-based visual control of differential drive vehicles with field-of-view constraints. In *IEEE International Conference on Robotics and Automation*, pages 4238–4244, 2007.

[10] P. Rives. Visual servoing based on epipolar geometry. In *IEEE/RSJ International Conference on Intelligent Robots and Systems*, volume 1, pages 602–607, 2000.

[11] G. L. Mariottini, D. Prattichizzo, and G. Oriolo. Epipole-based visual servoing for nonholonomic mobile robots. In *IEEE International Conference on Robotics and Automation*, pages 497–503, 2004.

[12] G. López-Nicolás, C. Sagüés, J.J. Guerrero, D. Kragic, and P. Jensfelt. Nonholonomic epipolar visual servoing. In *IEEE International Conference on Robotics and Automation*, pages 2378–2384, 2006.

[13] G. L. Mariottini, G. Oriolo, and D. Prattichizzo. Image-based visual servoing for nonholonomic mobile robots using epipolar geometry. *IEEE Transactions on Robotics*, 23(1):87–100, 2007.

[14] G. López-Nicolás. *Visual Control of Mobile Robots Through Multiple View Geometry*. PhD thesis, DIIS, University of Zaragoza, Spain, June 2008.

[15] J. Guldner V. Utkin and J. Shi. *Sliding Mode Control in Electromechanical Systems*. CRC Press, Boca Raton, 1999.

[16] A. Isidori. *Nonlinear Control Systems*. Springer, Great Britain, 1995.

[17] R. M Hirschorn. Output tracking through singularities. In *IEEE Conference on Decision and Control*, pages 3843–3848, 2002.

[18] S. Sastry. *Nonlinear Systems: Analysis, Stability and Control*. Springer, New York, 1999.